Thermal Structure of Mars' Middle and Upper Atmosphere: Understanding the Impacts of Dynamics and Solar Forcing

Emmaris Soto[1], Sonal Jain[2], J. Scott Evans[1], Justin Deighan[2], Nicholas M. Schneider[3], and Stephen Bougher[4]

[1]Computational Physics Inc., [2]Laboratory for Atmospheric and Space Physics, Univ. of Colorado, [3]Univ. of Colorado, [4]Climate and Space Sciences and Engineering Department, Univ. of Michigan

Abstract

Characterizing the present state of the Martian upper atmosphere is an important component in understanding the interactions of Mars with its space environment, atmospheric loss, and for missions to Mars that utilize the upper atmosphere for aerobraking maneuvers. The mesosphere (90-105 km) and thermosphere (170–190 km) provide the reservoir for atmospheric volatile evolution via numerous escape processes. Characterization of the thermal variability of Mars' upper atmosphere, including the mesosphere and thermosphere, is necessary to understand any present-day or historic escape rate. We report six years of dayside mesosphere and thermosphere temperatures obtained by the Imaging Ultraviolet Spectrograph [IUVS; McClintock et al. 2015] aboard the Mars Atmospheric and Volatile EvolutioN [MAVEN; Jakosky et al. 2015] spacecraft. Thermospheric temperatures show strong long-term variability associated with Martian season and solar cycle. Temperatures from both the Martian thermosphere and mesosphere show strong short-term variability indicating coupling from the lower atmosphere. The observed local time effect is strong in both upper and middle atmosphere temperatures. The thermosphere tends to be colder in the morning compared to the evening when temperatures are higher while mesospheric temperatures show cooling during both the dawn and dusk hours. Our analysis shows strong tidal activity during aphelion, whereas nonmigrating tides are suppressed during perihelion, possibly due to increased dust activity. Observations during the deep minimum of solar cycle 24 reveal that thermospheric temperatures are highly variable with respect to local time if solar forcing, Mars-Sun distance, and spatial effects are removed. We will discuss these results in the context of coupling between the lower and upper atmosphere of Mars.

Methodology

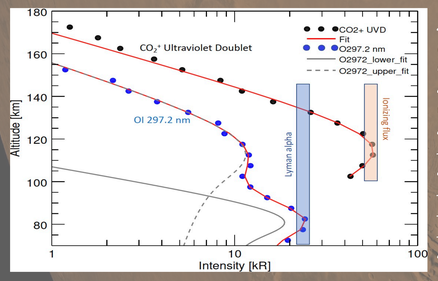

***Figure 1**: Solid black and blue circles show the intensity of CO_2+ UVD and OI 297.2 nm emissions from scan 2 of orbit 3108 (5 May 2016). The red curves show an empirical Chapman fit to the data. The final fit of OI 297.2 nm consists of two Chapman fits: one for the lower peak (solid grey line) and another for the upper peak (dashed grey line). The red and blue bars show the solar irradiance responsible for creating the main airglow layer and lower peak of OI 297.2 nm emission, respectively.*

MAVEN IUVS measures the mid-ultraviolet airglow between 180 and 340 nm at 1.2 nm resolution with a vertical resolution of 5 km. Limb scan observations constrained to solar zenith angles < 85° for daytime local solar times (LSTs, 6-18 h) from late October 2014 through September 2020 are utilized in this study. The observations span all latitudes and longitudes, and include inlimb, outlimb, and periapse limb scans. To extract temperatures, we use an empirical Chapman fit to CO_2^+ Ultraviolet Doublet (UVD; at 290 nm) and O I 297.2 nm emission intensities, respectively, to determine scale heights. With this method, we use an integral of parameterized volume emission rate (Eq. 1) to fit the measured intensity using a Levenberg-Marquardt least squares minimization algorithm.

$$I = 2\int_b^\infty \Pi_F \sigma\eta_0 exp\left(\frac{z_0 - z}{H} - \frac{\sigma_0\eta_0 H}{\cos(\chi)} e^{(z_0-z)/H}\right)\frac{rdz}{\sqrt{r^2-b^2}} \qquad \text{(Eq. 1)}$$

where Π_F accounts for solar flux and calibration factors; z is the altitude; b is the tangent altitude of the line of sight from the center of the planet; z_0 is the reference altitude, which is set at 130 km in this analysis; H is the scale height; r = R + z, where R is the radius of Mars; χ is the solar zenith angle; σ_0 is the photo-absorption cross section of UV photons and n_0 represents the CO_2 density at the reference altitude of z_0. The three parameters, viz., Π_F, H, and scaled density $\sigma_0\eta_0$ are allowed to vary during the fit. Figure 1 shows an example of the model fits (red curves) to IUVS CO_2^+ UVD and O I 297.2 nm data. For O I 297.2 nm, two Chapman fits are required to capture the double peak of the emission: one for the upper peak (dashed grey line) and one for the lower peak (solid grey line). Results presented here are determined from IUVS level 2 operational retrievals and level 1C version 13 revision 1 data products. Data from the Extreme Ultraviolet Monitor (EUVM) was also used to examine the role of EUV flux. The EUVM data set used in this analysis is the level 2 and 3 version 14 revision 1 data product. All data products are available on the NASA Planetary Data System and the LASP Data Science Center.

Please check out our digital poster for additional plots and details! Our publication is also available!

POSTER PAPER

Additional questions? Comments? Please don't hesitate to reach out!
Dr. Emmaris Soto
Computational Physics Inc.
8001 Braddock Rd Suite 210, Springfield, VA 22151
esoto@cpi.com

Key Insights & Results

- **These are the first long term (6 years) observations of Martian mesospheric and thermospheric temperatures (Figure 2) which show thermal variability in the thermosphere driven by Mars season, however, no such trend is present in the mesosphere (Figure 3).**
- **Thermospheric temperatures show dependence on Mars season, LST, and solar EUV (Figures 2 & 3).**
- **Coupling between the lower and upper atmosphere is indicated by non-migrating tides (Figure 4).**
- **Analysis of thermospheric temperatures during the deep solar minimum indicate that temperatures are highly variable with LST when solar forcing, Mars-Sun distance, and dust effects are removed (Figure 5).**

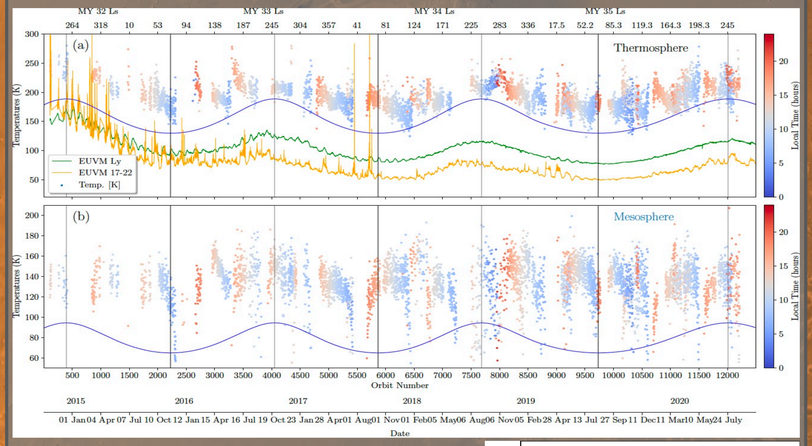

***Figure 2 (Above)**: Mean thermospheric and mesospheric temperatures (color-coded according to LST) per orbit inferred from the scale height (using Eq. 1) derived from IUVS observations of CO_2+ UVD emission profiles. The data from two channels (17-22 nm and Lyman alpha) of the Extreme Ultraviolet Monitor (EUVM) on MAVEN, which were taken simultaneously with the dayglow observations, are also plotted on the same graph with arbitrary scaling. The thin blue curve shows the inverse of the square of Mars radial distance from the Sun (with arbitrary scaling). The solar longitudes are plotted on the top x-axis along with labels indicating the Martian year (MY). Thin gray and black vertical lines show the location of perihelion and aphelion, respectively.*

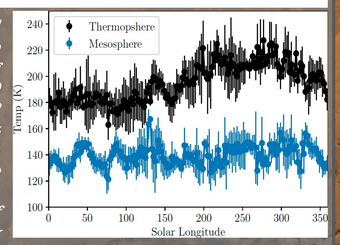

***Figure 3 (Above)**: Seasonal behavior of Martian thermosphere (black) and mesosphere (blue) temperatures.*

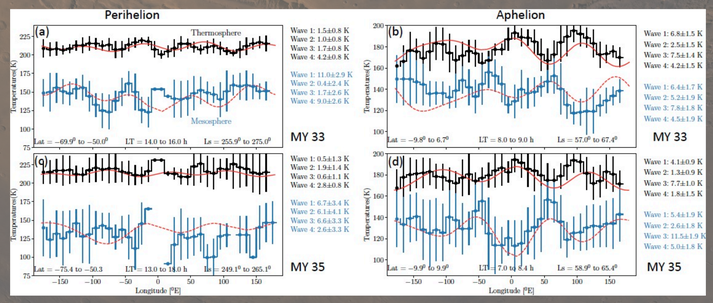

***Figure 4**: Harmonic fit to the temperatures retrieved during perihelion (6 No. - 6 Dec. 2016) and (9 July - 26 Aug. 2020) are shown in panels (a) and (c), with mean 17-22 nm irradiance of 2.5 x 10^{-4} and 2.2 x 10^{-4} W/m^2, respectively, and during aphelion (19 Oct. - 12 Nov. 2015) and (7 July - 23 Aug. 2019) are shown in panels (b) and (d) with a mean 17-22 nm irradiance of 2.4 x 10^{-4} and 1.2 x 10^{-4} W/m^2, respectively for for MY 33 and MY 35. Solid black and blue curves show the average temperature derived from CO_2+ UVD (at 170 km) and from the OI 297.2 nm lower peak (near 90 km) over 20 deg latitude bins along with their standard deviation. Red solid and dashed curves show the harmonic fit to the temperatures derived from UVD and OI 297.2 nm emissions, respectively. The wave amplitudes are shown next to the figure with black and blue text for the respective temperature harmonic fit. The latitude, local time, and solar longitude information is provided in each panel. (top) For solar max to moderate condition. (bottom) For solar minimum condition.*

Solar Minimum

We analyze the deep solar minimum period after solar cycle 24, constraining our analysis from mid-May 2019 through September 2020. The quiet solar activity period provides ideal conditions to decouple and quantify the effects of weaker parameters that may drive temperature variability in the upper atmosphere. During March 2020 Mars began its approach to perihelion (2.066x10^8 km); however, to mitigate the impact of variations in orbital distance we scale the temperatures using a power law to remove the Mars-Sun distance dependency. At the lowest order approximation, mesospheric temperatures behave approximately as the inverse square root of the Mars-Sun distance according to the Stefan-Boltzmann law and this behavior roughly propagates into the thermosphere.

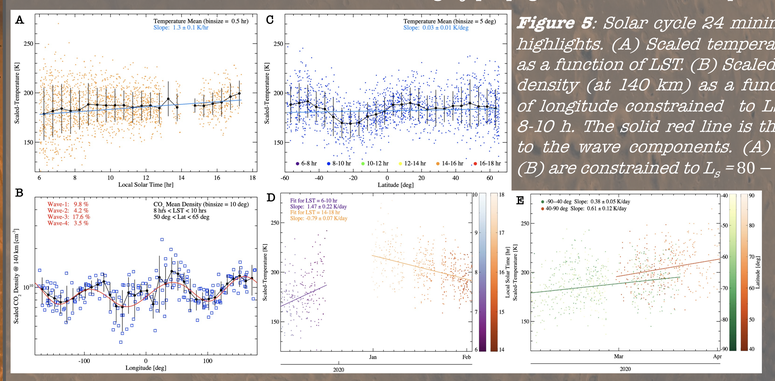

***Figure 5**: Solar cycle 24 minimum highlights. (A) Scaled temperature as a function of LST. (B) Scaled CO_2 density (at 140 km) as a function of longitude constrained to LST = 8-10 h. The solid red line is the fit to the wave components. (A) and (B) are constrained to L_S = 80 – 105° and 10° ≤ Lat ≤ 70°. (C) Scaled temperature as a function of latitude for LST = 8-10 h constrained to L_S < 130°. In (A) - (C) the data and corresponding 1- error bars are shown in black and the linear fit is shown in light blue. (D) Scaled temperature time series (as a function of Julian day) color-coded with respect to LST. Linear fits are shown in purple for 6-10 h and orange for 14-18 h LST bins. The data is constrained to 120° ≤ L_S ≤ 150° and −30° ≤ Lat ≤ 10°. (E) Scaled temperature time series (as a function of Julian day) color-coded with respect to latitude bin; orange/red for northern hemisphere and yellow/green for southern hemisphere. Data is constrained to 160° ≤ L_S ≤ 190° and LST = 10-12 h.*

- **(A)** Temperature increases from dawn hours to dusk at northern latitudes.
- **(B)** We find wave-4 structure in the CO_2 densities with a dominant wave-3 component.
- **(C)** Wave structure appears with respect to latitude, which may be attributed to meridional circulation.
- **(D)** Temperatures in the 6-10 h bin increase as LST decreases while temperatures in the 14-18 h bin decrease as LST decreases.
- **(E)** The temperatures in the northern hemisphere are warmer than at southern latitudes and appear shifted by ~10 K.

Discussion

- **This study reveals that the majority of the thermal structure in the highly variable thermosphere is modulated by Mars season (warmer and cooler mean temperatures during perihelion and aphelion, respectively) and is coupled with solar EUV forcing (solar insolation changes by 40% from perihelion to aphelion).**
- **Mesospheric temperatures show no systematic dependence on solar EUV forcing, which is to be expected since this layer is below the EUV heating region, or Mars season (Figures 2 & 3), rather the large variability in the mesosphere is attributed to the effects from coupling with the lower atmosphere.**
- **Temperatures from the middle and upper atmospheres show strong dependence on LST (Figure 2). Thermospheric temperatures tend to be warmer during the afternoon hours compared to morning due to the strong solar EUV absorption in the afternoon.**
- **The substantially reduced variability in solar irradiance during solar minimum and scaling of temperatures to remove seasonal dependence reveals stronger effects from changes in LST than latitude on thermospheric temperatures (Figure 5, with variations up to 50% greater with respect to changes in LST).**

The large orbit to orbit variabilities observed in the thermosphere indicate that the upper atmosphere of Mars is coupled strongly to the lower atmosphere by dynamics (and so is the mesosphere). To understand the coupling between these layers, we fit the longitudinal tidal components (Fig. 4) and typically find a dominant wave-4 and wave-1 component in thermospheric and mesospheric temperatures, respectively, during perihelion and dominant wave-3 component in both during aphelion. Although solar activity was greater during aphelion of MY 33 there is still strong wave activity which indicates that solar forcing may not be responsible for suppressing wave activity during perihelion of MY 35, rather high dust activity may cause the repression of non-migrating tides [Guzewich et al. 2014].